Critical parameters from trap-size scaling in trapped particle systems

Giacomo Ceccarelli,[1] Christian Torrero,[2] and Ettore Vicari[1]
[1] *Dip. di Fisica dell'Università di Pisa and INFN, Largo Pontecorvo 2, I-56127 Pisa, Italy and*
[2] *Dip. di Fisica dell'Università di Parma and INFN, viale Usberti 7/A, I-43124 Parma, Italy*
(Dated: November 27, 2012)

We investigate the critical behavior of trapped particle systems at the low-temperature superfluid transition. In particular, we consider the three-dimensional Bose-Hubbard model in the presence of a trapping harmonic potential coupled with the particle density, which is a realistic model of cold bosonic atoms in optical lattices. We present a numerical study based on quantum Monte Carlo simulations, analyzed in the framework of the trap-size scaling (TSS).

We show how the critical parameters can be derived from the trap-size dependences of appropriate observables, matching them with TSS. This provides a systematic scheme which is supposed to exactly converge to the critical parameters of the transition in the large trap-size limit. Our numerical analysis may provide a guide for experimental investigations of trapped systems at finite-temperature and quantum transitions, showing how critical parameters may be determined by looking at the scaling of the critical modes with respect to the trap size, i.e. by matching the trap-size dependence of the experimental data with the expected TSS Ansatz.

PACS numbers: 05.70.Fh,67.85.-d,67.25.dj,05.30.Jp

I. INTRODUCTION

The theory of critical phenomena[1,2] at phase transitions generally applies to homogenous systems. However, homogeneous conditions are often an ideal limit of experimental conditions. Thus, the study of the effects of inhomogeneous features is often essential to achieve a correct interpretation of the experimental data at the transition between different phases, in order to obtain reliable estimates of the critical parameters, such as the critical temperature, universal critical exponents, etc.

In this paper we focus on quantum systems of interacting particles in the presence of an external space-dependent potential coupled to the particle density, which effectively traps the particles within a limited region of space. The presence of a harmonic trap is a common feature of the experimental realizations of the Bose-Einstein condensation (BEC) in diluted atomic vapors[3] and experiments of cold atoms in optical lattices created by laser-induced standing waves[4,5], which have provided a great opportunity to investigate the interplay between quantum and statistical effects in particle systems.

The critical behavior arising from the formation of BEC has been investigated experimentally in a trapped atomic system[6], observing an increasing correlation length compatible with what expected at a continuous transition. However, the inhomogeneity due to the trapping potential drastically changes, even qualitatively, the general features of the behavior at a phase transition. For example, the correlation functions of the critical modes do not develop a diverging length scale in a trap. Nevertheless, even in the presence of the trap, and in particular when the trap gets large, we may still observe a critical regime although distorted by the presence of the trap. In experiments of trapped particle systems aimed to investigate their many-body critical behaviors at quantum and finite-temperature phase transitions, an accurate determination of the critical parameters, such as the critical temperature, critical exponents, etc..., calls for a quantitative analysis of the trap effects. This issue has been much discussed within theoretical and experimental investigations, see e.g. Refs. 7–41.

Around the transition point, the critical behavior in trapped systems is expected to show a power-law scaling with respect to the trap size, which we call trap-size scaling[17,23] (TSS), controlled by the universality class of the phase transition of the homogenous system. TSS has some analogies with the standard finite-size scaling (FSS) theory for homogenous systems[42–44], with two main differences: the inhomogeneity due to the space-dependence of the external field, and a nontrivial power-law dependence of the correlation length ξ when increasing the trap size l at the critical point, i.e. $\xi \sim l^\theta$ where θ is the universal *trap* exponent.

In this paper we show how TSS can be exploited to determine the critical parameters of trapped particle systems, by analyzing the trap-size dependence of observables related to the critical modes around the center of the trap. The main advantage of this approach is that it is supposed to be exact in the large trap-size limit, thus providing a systematic scheme to control and improve the accuracy of the results, without appealing to further assumptions and approximations, such as mean-field and local-density approximations. As we shall see, the method resembles standard FSS techniques, which are routinely used to obtain accurate estimates of the critical parameters in homogeneous systems, by looking at the asymptotic scaling behavior with respect to the size of the system, see, e.g., Refs. 45,46.

We investigate this issue at the finite-temperature superfluid transition of the three-dimensional (3D) Bose-Hubbard (BH) model[47], which is particularly relevant for cold-atom experiments because it describes bosonic atoms in optical lattices[48]. For this purpose we present

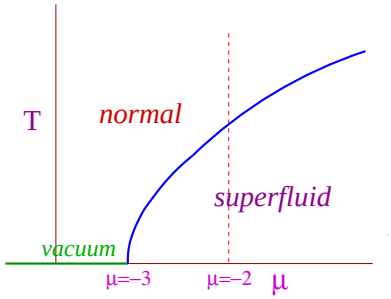

FIG. 1: (Color online) Sketch of the T-μ phase diagram of the 3D BH model (1) in the hard-core $U \to \infty$ limit. The superfluid transition line starts at $(T = 0, \mu = -3)$, which is the location of a quantum transition from the vacuum state to the superfluid phase, and ends at another quantum transition at $(T = 0, \mu = 3)$ (not shown in the figure) between the superfluid and Mott phases. The dashed line at $\mu = -2$ shows the line along which we numerically investigate the critical behavior.

a numerical analysis based on quantum Monte Carlo (QMC) simulations of the 3D BH model with an external harmonic potential coupled to the particle density.

This study may be useful for experimental investigations of trapped systems at finite-temperature and quantum transitions, suggesting some effective recipes to determine the critical parameters from the scaling of the observables related to the critical modes with respect to the trap size, i.e. by matching the trap-size dependence of the experimental data with the expected TSS Ansatz, similarly to experiments probing FSS behavior in ^{4}He at the superfluid transition[44].

The paper is organized as follows. In Sec. II we present the general features of the TSS in trapped bosonic particle systems at the finite-temperature superfluid transition driven by the formation of a BEC, such as those described by the 3D BH model. Sec. III presents a numerical study of the superfluid transition of the 3D BH model in the hard-core limit, using standard FSS techniques, which allows us to verify the 3D XY universality class of the critical behavior, and to accurately determine the critical point. In Sec. IV we show how the critical parameters can be estimated by a TSS analysis of numerical QMC data of the trapped BH model. Finally, in Sec. V we draw our conclusions. App. A reports some details of the computation of the trap exponent θ at the 3D superfluid transition of bosonic systems.

II. TSS AT THE SUPERFLUID TRANSITION OF THE 3D BOSE-HUBBARD MODEL

A. The phase diagram of the 3D BH model

Systems of bosonic atoms in optical lattices can be modeled by the 3D BH model[4,48], defined by the Hamiltonian[47]

$$H_{\rm BH} = -\frac{J}{2}\sum_{\langle ij\rangle}(b_i^\dagger b_j + b_j^\dagger b_i) + \\ + \frac{U}{2}\sum_i n_i(n_i-1) - \mu\sum_i n_i\,, \quad (1)$$

where b_i is the bosonic operator, $n_i \equiv b_i^\dagger b_i$ is the particle density operator, and the sums run over the bonds $\langle ij\rangle$ and the sites i of a cubic lattice. The basic observables are related to the particle density

$$\rho(\mathbf{x}) \equiv \langle n_{\mathbf{x}}\rangle, \quad (2)$$

and the correlation functions of the bosonic field and the particle density,

$$G_b(\mathbf{x},\mathbf{y}) \equiv \langle b_{\mathbf{x}}^\dagger b_{\mathbf{y}}\rangle, \quad (3)$$
$$G_n(\mathbf{x},\mathbf{y}) \equiv \langle n_{\mathbf{x}} n_{\mathbf{y}}\rangle - \langle n_{\mathbf{x}}\rangle\langle n_{\mathbf{y}}\rangle. \quad (4)$$

In actual experiments the particle density and its correlations, such as G_n, can be measured by the so-called *in situ* density image techniques, see e.g. Refs. 14,49,50. Some information on the correlation function G_b, and in particular the related momentum distribution

$$n(\mathbf{k}) = \sum_{\mathbf{x},\mathbf{y}} e^{i\mathbf{k}(\mathbf{x}-\mathbf{y})} G_b(\mathbf{x},\mathbf{y}), \quad (5)$$

can be inferred from the interference patterns of absorption images after a time-of-flight period in the large-time ballistic regime, see e.g. Ref. 4.

The T-μ phase diagram of the 3D BH model presents a finite-T transition line separating the normal-fluid phase and the low-temperature superfluid phase. The finite-T superfluid transition is characterized by the accumulation of a macroscopic number of bosonic atoms in a single quantum state, giving rise to the BEC. The condensate wave function naturally provides the complex order parameter $\psi(x)$ of the phase transition and its relevant U(1) symmetry. These global features characterize the 3D XY universality class which describes the universal critical behavior of a wide class of systems, see, e.g., Ref. 45. Numerical studies of the phase diagram of the 3D BH model are reported in Refs. 41,51.

In Fig. 1 we sketch the T-μ phase diagram of the 3D BH model in the hard-core $U \to \infty$ limit, implying that the particle number n_i per site is restricted to the values $n_i = 0, 1$. The finite-T transition line connects two $T = 0$ quantum critical points at $\mu = \pm 3$. The $T = 0$ quantum transition at $\mu = -3$ separates the vacuum state and the superfluid phase, while the one at $\mu = 3$ separates the superfluid phase from a Mott phase. In both cases the quantum critical behavior is essentially mean field in three spatial dimensions[47], see also Ref. 52.

The critical behavior described by the 3D XY universality class is characterized by two relevant parameters τ and h, associated with the temperature T, i.e.,

$\tau \sim T/T_c - 1$, and the external field h coupled to the order parameter. Their renormalization-group (RG) dimensions, $y_\tau = 1/\nu$ and $y_h = (5-\eta)/2$ respectively, are related to the critical exponent ν of the correlation length and to the exponent η describing the power-law decay of the two-point function of the order parameter at T_c. The critical exponents ν and η are known with great accuracy from theoretical calculations, see, e.g., the results reported in Refs. 45,53, and experiments at the ^{4}He superfluid transition[54]. Recent theoretical estimates of the critical exponents are[55,56]

$$\nu = 0.6717(1), \qquad \eta = 0.0381(2). \tag{6}$$

B. TSS in the presence of the trap

A common feature of the experiments with cold atoms[4] is the presence of an external potential V coupled to the particle density, which traps the particles within a limited space region. In experiments V is usually effectively harmonic. We consider a harmonic rotational-invariant potential

$$V(r) = v^2 r^2, \tag{7}$$

where $r \equiv |\mathbf{x}|$ is the distance from the center of the trap, which we locate at the origin of the axis, $\mathbf{x} = 0$. This trapping force gives rise to a further term in the Hamiltonian:

$$H_{\rm tBH} = H_{\rm BH} + \sum_i V(r_i) n_i. \tag{8}$$

Far from the origin the potential $V(r)$ diverges, therefore $\langle n_i \rangle$ vanishes and the particles are trapped. We define the trap size by

$$l \equiv \sqrt{J}/v. \tag{9}$$

This definition naturally arises[4,7,9,30] when we consider the *thermodynamic* limit, which is generally defined by the limit $N, l \to \infty$ keeping N/l^3 fixed (N is the number of particles), and it is equivalent to introducing the chemical potential μ, as in Eq. (1). In the following, we set $J = 1$ so that $l = 1/v$. We consider the model at fixed chemical potential μ, so we will skip its dependence in the following formulas.

In the presence of a harmonic trap, the large trap-size behavior at the transition can be described in the framework of TSS. The trapping potential (7) coupled to the particle density, as in Eq. (8), significantly affects the critical modes, introducing another length scale (9). Within the TSS framework[17,23], the scaling law of the singular part of the free-energy density around the center of the trap can be written as

$$F_{\rm sing}(\mathbf{x}, T, h) = l^{-3\theta} \mathcal{F}(r l^{-\theta}, \tau l^{\theta y_\tau}, h l^{\theta y_h}). \tag{10}$$

where y_τ and y_h are the RG dimensions reported at the end of Sec. II A, and θ is the trap exponent. TSS implies that at the critical point ($\tau = 0$) the correlation length ξ of the critical modes is finite, but increases as $\xi \sim l^\theta$ with increasing the trap size l. The trap exponent can be inferred by a renormalization-group (RG) analysis of the perturbation induced by the external trapping potential coupled to the particle density. We obtain[17]

$$\theta = \frac{2\nu}{1+2\nu} = 0.57327(4). \tag{11}$$

The derivation is outlined in App. A.

The TSS equations for the observables and correlation functions provide an effective description of the critical behavior around the center of the trap, and, in particular, of the interplay between the temperature and the confining potential. At the superfluid transition and around the center of the trap, the one-particle correlation function G_b behaves as

$$G_b(\mathbf{x}, \mathbf{y}) \approx l^{-(1+\eta)\theta} \mathcal{G}_b(\mathbf{x} l^{-\theta}, \mathbf{y} l^{-\theta}, \tau l^{\theta/\nu}), \tag{12}$$

and the particle-density correlation G_n as

$$G_n(\mathbf{x}, \mathbf{y}) \approx l^{-2y_n\theta} \mathcal{G}_n(\mathbf{x} l^{-\theta}, \mathbf{y} l^{-\theta}, \tau l^{\theta/\nu}), \tag{13}$$

where y_n is the RG dimension of the density operator

$$y_n = 3 - 1/\nu = 1.5112(2). \tag{14}$$

Analogous scaling relations can be inferred for other correlations.

In our TSS analyses we consider the trap susceptibility χ_t defined as

$$\chi_t = \sum_{\mathbf{x}} G_b(\mathbf{0}, \mathbf{x}) \tag{15}$$

(we distinguish it from a generic susceptibility because χ_t is the space integral of the correlations with the center of the trap), and the trap correlation length ξ_t defined from the second moment of $G_b(0, \mathbf{x})$, i.e.

$$\xi_t^2 = \frac{1}{6\chi_t} \sum_{\mathbf{x}} |\mathbf{x}|^2 G_b(0, \mathbf{x}). \tag{16}$$

According to TSS, they are expected to behave as

$$\chi_t \approx l^{(2-\eta)\theta} \mathcal{X}(\tau l^{\theta/\nu}), \tag{17}$$

$$\xi_t \approx l^\theta \mathcal{R}(\tau l^{\theta/\nu}). \tag{18}$$

Note however that any length scale ξ extracted from the critical modes is expected to show the same TSS as ξ_t.

The above TSS equations provide the asymptotic dependence on the trap size l. Scaling corrections are generally expected to be $O(l^{-\omega\theta})$ where $\omega = 0.785(20)$ is the scaling-correction exponent of the 3D XY universality class[45,53,55], thus

$$\omega\theta = 0.45(1). \tag{19}$$

We remark that the lattice structure of the BH model does not play any particular role in the derivation of the

TSS formulas, i.e. the microscopic details of the model are irrelevant in the TSS limit. Therefore, the above TSS equations apply to a wide class of models, i.e. to general 3D interacting bosonic systems at the transition driven by the BEC, thus also including the atomic system experimentally investigated in Ref. 6.

We also mention that an analogous TSS behavior applies to the $T = 0$ quantum superfluid-to-Mott phase transition of the 2D BH model (1) at fixed integer density[23], which belongs to the same 3D XY universality class[47].

III. FINITE-SIZE SCALING ANALYSIS

Before studying the effect of an external space-dependent trapping potential, we present a finite-size scaling (FSS) analysis of quantum Monte Carlo (QMC) simulations of the homogenous BH model (1), with periodic boundary conditions. In particular, we consider the $U \to \infty$ hard-core limit of the BH model at fixed chemical potential $\mu = -2$, and vary the temperature along the dashed line sketched in Fig. 1. The QMC simulations are performed using the stochastic series expansion algorithm with the directed operator-loop technique[57,58].

A. Observables and their FSS

We compute the particle density ρ, the one-particle correlation function $G_b(\mathbf{x}, \mathbf{y})$,[59] cf. Eq. (3), and the particle-density correlation $G_n(\mathbf{x}, \mathbf{y})$, cf. Eq. (4). Due to translation invariance, they only depend on the difference of the arguments, i.e. $G_\#(\mathbf{x}, \mathbf{y}) \equiv G_\#(\mathbf{x} - \mathbf{y})$.

We consider the susceptibility

$$\chi = \sum_{\mathbf{x}} G_b(\mathbf{x}), \tag{20}$$

which is the zero-momentum component of the Fourier transform of G_b,

$$\widetilde{G}_b(\mathbf{k}) = \sum_{\mathbf{x}} e^{i\mathbf{k}\cdot\mathbf{x}} G_b(\mathbf{x}). \tag{21}$$

Note that, due to translation invariance, $\widetilde{G}_b(\mathbf{k})$ coincides with the so-called momentum distribution defined by the double sum (5), apart from a volume factor. When the system has periodic boundary conditions, the second-moment correlation length ξ is conveniently defined by

$$\xi^2 \equiv \frac{1}{4\sin^2(p_{\min}/2)} \frac{\widetilde{G}_b(\mathbf{0}) - \widetilde{G}_b(\mathbf{p})}{\widetilde{G}_b(\mathbf{p})}, \tag{22}$$

where $\mathbf{p} = (p_{\min}, 0, 0)$, $p_{\min} \equiv 2\pi/L$. We also consider the so-called helicity modulus[55,60] Υ, which is related to the spin stiffness in spin models[61], and to the superfluid density in particle systems[42,62]. In QMC simulations using the stochastic series expansion algorithm, Υ is obtained from the linear winding number w_i along the i^{th} direction,

$$\Upsilon = \frac{\langle w_i^2 \rangle}{L}, \qquad w_i = \frac{N_i^+ - N_i^-}{L}, \tag{23}$$

where N_i^+ and N_i^- are the number of non-diagonal operators which move the particles respectively in the positive and negative i^{th} direction.

FSS predicts the following asymptotic scaling laws of the one-particle and particle density correlation functions for $r \equiv |\mathbf{x}| > 0$:

$$G_b(\mathbf{x}) \approx L^{-1-\eta} \mathcal{G}_b(r/L, \tau L^{1/\nu}), \tag{24}$$

$$G_n(\mathbf{x}) \approx L^{-2y_n} \mathcal{G}_n(r/L, \tau L^{1/\nu}), \tag{25}$$

where $\tau \equiv T/T_c - 1$. Thus, the susceptibility χ behaves as

$$\chi = L^{2-\eta} \left[g(\tau L^{1/\nu}) + L^{-\omega} g_\omega(\tau L^{1/\nu}) + ... \right], \tag{26}$$

where we have also included the leading $O(L^{-\omega})$ scaling corrections, and $\omega = 0.785(20)$[45,53,55] is the critical exponent controlling the leading scaling corrections in the 3D XY universality class. The dots indicate further scaling corrections suppressed by higher powers of $1/L$. The scaling functions g and g_ω are universal apart from a multiplicative constant (since χ is not RG invariant, $g(0)$ is not universal) and a rescaling of the argument.

We consider the dimensionless RG invariant quantities

$$R_\xi \equiv \xi/L, \qquad R_\Upsilon \equiv \Upsilon L. \tag{27}$$

According to the FSS theory[42,43,45], they behave as (see, e.g., Ref. 55)

$$R = f(\tau L^{1/\nu}) + L^{-\omega} f_\omega(\tau L^{1/\nu}) + ..., \tag{28}$$

around T_c and in the large L limit. f and f_ω are scaling functions. In particular the leading one f is universal (although it depends on the shape of the volume and the choice of the boundary conditions), i.e. it is independent of the particular model within the universality class, apart from a trivial rescaling of the argument. Thus, $R^* \equiv f(0)$ is universal. For cubic-shaped lattices with periodic boundary conditions, the universal infinite-volume limit of R_ξ and R_Υ at $T = T_c$ are known with great accuracy:[55] $R_\xi^* = 0.5924(4)$ and $R_\Upsilon^* = 0.516(1)$.

B. FSS of QMC data

We study the FSS of the observables defined above in cubic L^3 lattices, up to $L = 32$ (up to $L = 24$ for observables related to the one-particle correlation function G_b), with periodic boundary conditions.

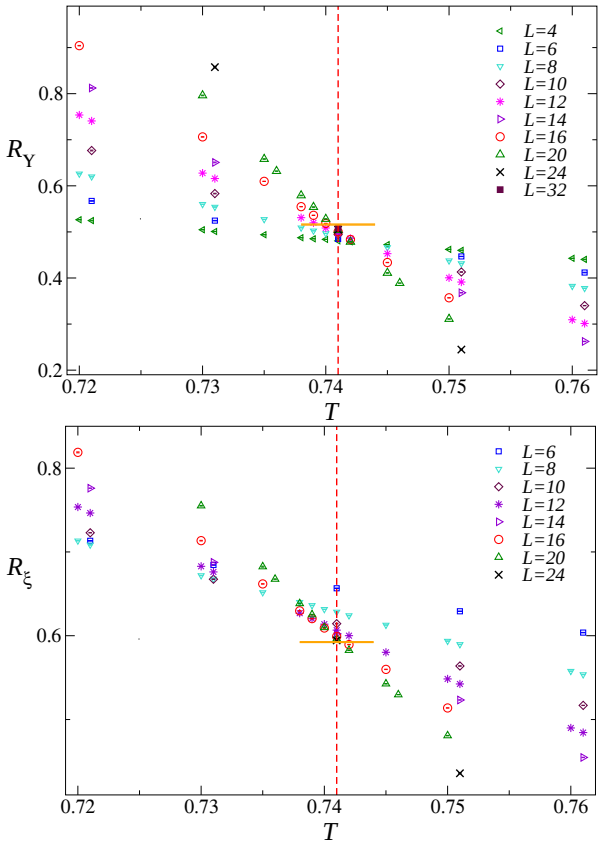

FIG. 2: (Color online) QMC data of $R_\xi \equiv \xi/L$ (bottom) and $R_\Upsilon \equiv \Upsilon L$ (top) for the 3D homogenous BH model (1) with periodic boundary conditions. The vertical dotted line shows our final estimate of T_c, i.e. $T_c = 0.7410(1)$. The horizontal segments around the crossing point indicate the universal asymptotic values[55] $R^*_\xi = 0.5924(4)$ and $R^*_\Upsilon = 0.516(1)$ at T_c.

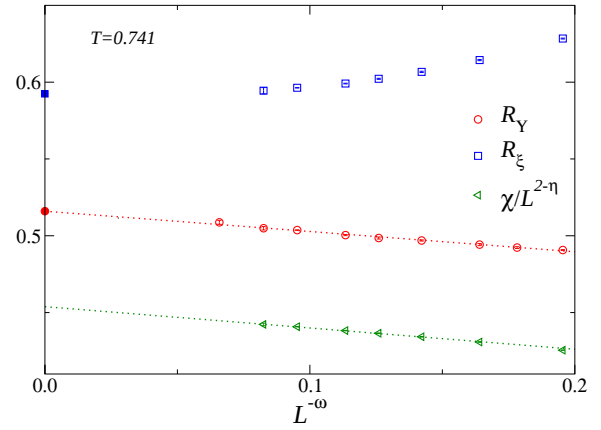

FIG. 3: (Color online) Data of R_Υ, R_ξ and $\chi/L^{2-\eta}$ at T_c versus $L^{-\omega}$ with $\omega = 0.785$. In the case of R_Υ and R_ξ we also show (by full symbols) their universal $L \to \infty$ limit: $R^*_\Upsilon = 0.516(1)$ and $R^*_\xi = 0.5924(4)$. The dotted lines show linear fits of the data of R_Υ and $\chi/L^{2-\eta}$. In the case of R_ξ, higher-order scaling corrections appear also important.

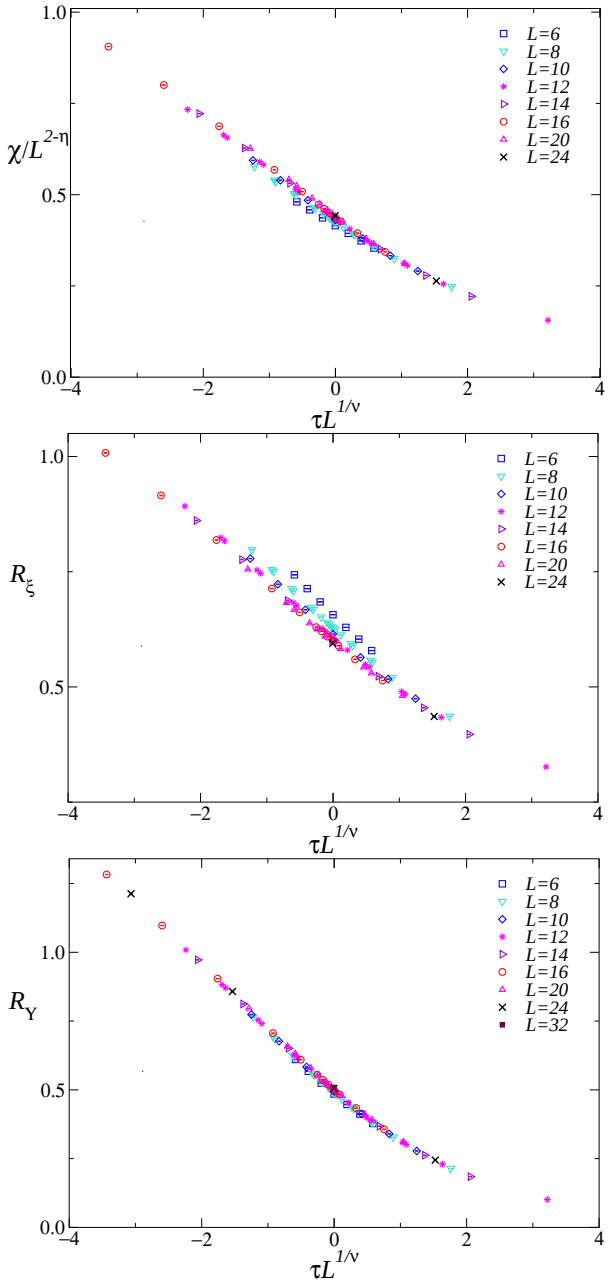

FIG. 4: (Color online) R_Υ (bottom), R_ξ (middle), and $\chi/L^{2-\eta}$ (top) versus $\tau L^{1/\nu}$ with $\tau \equiv T/T_c - 1$ and $T_c = 0.7410$, for homogenous 3D BH model with periodic boundary conditions

In Fig. 2 we show the QMC results for R_ξ and R_Υ. Their sets of data for different lattice sizes show a clear evidence of a crossing point, whose location is expected to converge to T_c in the large L limit, according to Eq. (28). Moreover, the values of R_ξ and R_Υ at the crossing point are consistent with the asymptotic universal values R^*_ξ and R^*_Υ reported above. The small deviations appear to decrease with increasing the lattice size; they are explained by the presence of $O(L^{-\omega})$ corrections, see Eq. (28) and also below. An analogous crossing point is

shown by the data of the ratio $\chi/L^{2-\eta}$.

In order to derive an estimate of T_c, we fit the data to the Ansatz

$$R = R^* + \sum_{i=1}^{n} a_i \tau^i L^{i/\nu} + L^{-\omega} \sum_{j=0}^{m} b_j \tau^j L^{j/\nu}, \qquad (29)$$

obtained by expanding Eq. (28) around $\tau = 0$. The best estimate of T_c is obtained from the data of R_Υ. Sufficiently close to T_c, for data with $|R_\Upsilon/R^*_\Upsilon - 1| \lesssim 0.1$ say, the first terms of the sums [i.e. setting $n = 1$ and $m = 0$ in Eq. (29)] provide already good fits keeping the known universal quantities ν, ω and R^*_Υ fixed (in this respect the $O(L^{-\omega})$ scaling correction term is necessary to achieve fits with acceptable χ^2/d.o.f). For example the fit of the data for $L \geq 10$ gives $T_c = 0.74103(1)$ with χ^2/d.o.f ≈ 1.4. We consider

$$T_c = 0.7410(1) \qquad (\mu = -2), \qquad (30)$$

as our final estimate of T_c, where the error includes the statistical errors of the fits, and takes into account the dependence of the results on the choice of the Ansatz and the interval of values of T around the transition allowed in the fit. Further subleading scaling corrections are controlled by increasing the minimum value $L_{\rm min}$ of L of the data allowed in the fits. The analysis of the data of R_ξ gives consistent results, but less precise because they are apparently affected by larger scaling corrections.

Fig. 3 shows data of R_ξ, R_Υ and $\chi/L^{2-\eta}$ at $T_c = 0.741$, plotted versus $L^{-\omega}$ which is the expected order of the leading scaling corrections. As expected R_ξ and R_Υ converge to their universal values R^*_Υ and R^*_ξ. The approach of R_Υ and $\chi/L^{2-\eta}$ is approximately linear with respect to $L^{-\omega}$, while in the case of R_ξ also higher-order scaling corrections appear significant for the available lattice sizes.

Fig. 4 reports the QMC data of R_Υ, R_ξ and $\chi/L^{2-\eta}$ versus $\tau L^{1/\nu}$ with $\tau \equiv T/T_c - 1$. They show the asymptotic collapse of the data along a universal curve, apart from small scaling corrections which get suppressed with increasing L. Fig. 5 shows the data of the one-particle correlation function G_b at T_c, which are consistent with the expected asymptotic scaling behavior reported in Eq. (24).

In conclusion, the above FSS analysis of the QMC data of the 3D hard-core BH model at $\mu = -2$ definitely confirms that its superfluid transition belongs to the 3D XY universality class, and provides an accurate determination of the (nonuniversal) critical temperature, cf. Eq. (30).

C. Finite-size dependence of the particle density and its correlators

The behaviors of the particle density, the compressibility, and the particle-density correlators around the transition are particularly interesting because they can be directly investigated experimentally[10,14,49,63,64], for example by in *situ* density image techniques. Therefore we report a detailed analysis of their data.

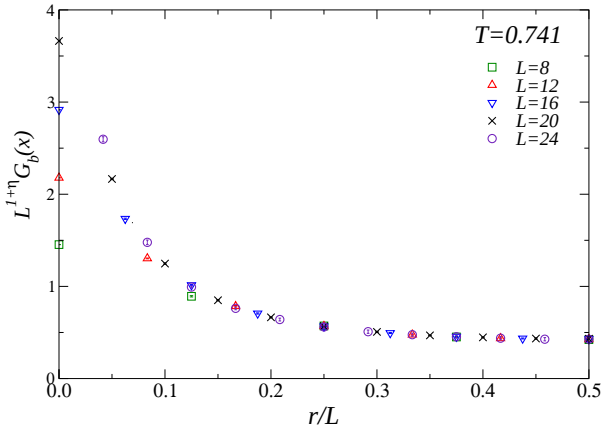

FIG. 5: (Color online) $L^{1+\eta}G_b(\mathbf{x})$ vs. r/L (where $r \equiv |\mathbf{x}|$) at $T = T_c$ for homogenous BH systems with periodic boundary conditions. The data show the expected scaling behavior (24).

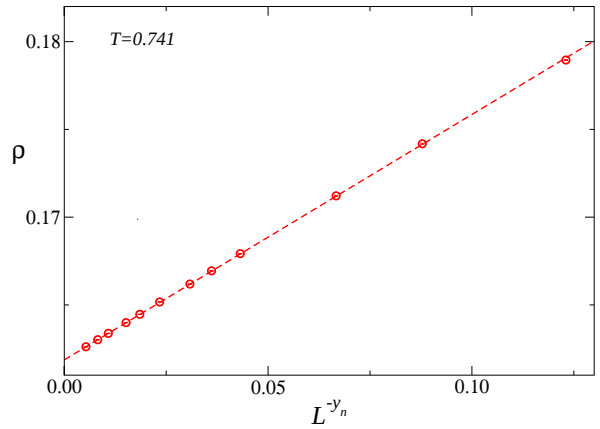

FIG. 6: (Color online) The particle density at T_c of the 3D homogenous BH model. The dashed line shows a linear fit of the data to $\rho_0 + c\,L^{-y_n}$, with $\rho_0 = 0.16187(1)$ and $c = 0.140(1)$.

The periodic boundary conditions preserve translation invariance, which implies that the particle density $\rho(\mathbf{x})$ is independent of $\mathbf{x}$, thus

$$\rho(\mathbf{x}) \equiv \rho = \frac{1}{L^3}\langle \hat{N} \rangle, \qquad \hat{N} = \sum_{\mathbf{x}} n_{\mathbf{x}}. \qquad (31)$$

Its behavior around the transition point is analogous to that of the energy density in spin systems, see e.g. Ref. 55, thus

$$\rho \approx f_a(\tau) + L^{-y_n} f_s(\tau L^{1/\nu}) \qquad (32)$$

at fixed chemical potential, where f_a is a nonuniversal analytic function of τ (and μ), y_n is the RG dimension of the particle density operator n_x, cf. Eq. (14), and f_s is a universal function apart from a factor and a rescaling of

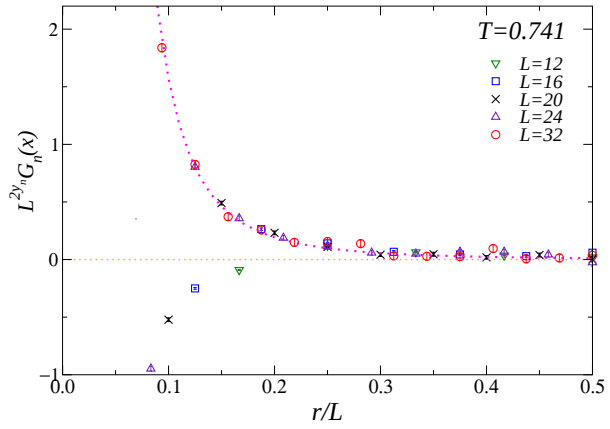

FIG. 7: (Color online) $L^{2y_n}G_n(x)$ vs. r/L at $T = T_c$ for homogenous systems with periodic boundary conditions. The dotted line sketches the expected asymptotic behavior $G_n(\mathbf{x}) \sim r^{-2y_n}$ at small $r \equiv |\mathbf{x}|$.

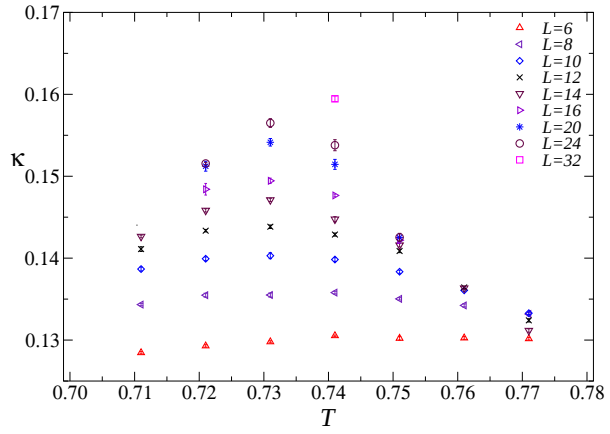

FIG. 8: (Color online) QMC data of the compressibility κ, cf. Eq. (34).

its argument. This behavior is clearly shown by the data at T_c, which are well approximated by the asymptotic formula

$$\rho \approx \rho_0 + c\, L^{-y_n}, \tag{33}$$

as shown by Fig. 6. A linear fit to (33) gives $\rho_0 = 0.16187(1)$.

Fig. 7 reports data of the particle-density correlation function at T_c. They show the expected scaling behavior, obtainable from Eq. (25) setting $\tau = 0$. Note that it develops for positive values of G_n, while the negative data at small distance are pushed toward the origin, not contributing to the scaling behavior. The space integral of G_n gives the compressibility

$$\kappa \equiv \frac{\partial \rho}{\partial \mu} = \sum_{\mathbf{x}} G_n(\mathbf{x}) = \frac{1}{L^3}\left(\langle \hat{N}^2\rangle - \langle \hat{N}\rangle^2\right). \tag{34}$$

Its scaling behavior is complicated by the sum around $\mathbf{x} = 0$, which gives rise to a nonuniversal analytic contribution, analogously to the specific heat in ^{4}He, see e.g.

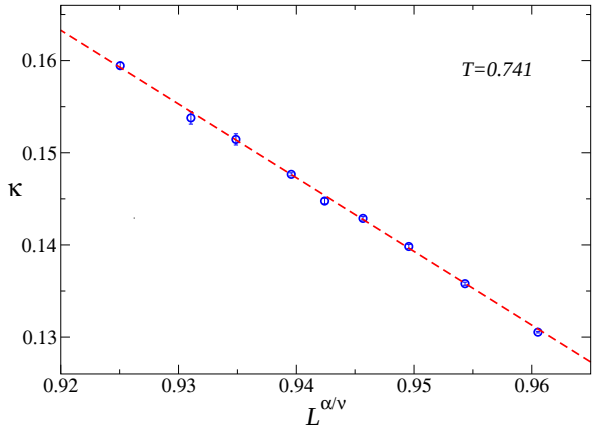

FIG. 9: (Color online) QMC data of the compressibility κ at T_c. The dashed line shows a linear fit to the predicted asymptotic behavior $a + bL^{\alpha/\nu}$; in particular, the data for $L \geq 8$ give $a = 0.90(1)$ and $b \approx -0.80(1)$ with χ^2/d.o.f. ≈ 1.1.

Ref. 45. Indeed, we expect

$$\kappa \approx g_a(\tau) + L^{\alpha/\nu} g_s(\tau L^{1/\nu}), \tag{35}$$

where α is the specific heat exponent $\alpha = -0.0151(3)$,[55] g_a is a nonuniversal analytic function of τ, and g_s is a universal function apart from a factor and a rescaling of the argument. Notice that, since $\alpha < 0$, the nonuniversal analytic term provides the leading behavior for $L \to \infty$. Fig. 8 shows the data of the compressibility. They hint at the typical λ shape expected in the infinite-volume limit, which also characterizes the specific heat at the superfluid transition of ^{4}He, see e.g. Refs. 44,54. At T_c they show the asymptotic scaling behavior

$$\kappa = a + b\, L^{\alpha/\nu}, \tag{36}$$

see Fig. 9. Linear fits of the available data at T_c, up to $L = 32$, gives $a \approx 0.90$ and $b \approx -0.80$.

IV. CRITICAL PARAMETERS FROM TSS

We now consider the 3D BH model in the presence of a trapping potential, as described by the Hamiltonian (8). We present results of QMC simulations of the 3D hard-core BH model at $\mu = -2$ for several values of the trap size l, up to $l = 14$. The trap is centered in the middle of a cubic L^3 lattice, with odd L and open boundary conditions. More details on the practical implementation of QMC simulations of trapped systems can be found in Refs. 37,39.

The lattice size L is taken sufficiently large to effectively reproduce the infinite-volume limit, i.e., so that the residual finite-size effects can be considered negligible compared with the statistical errors. This is checked by comparing results at fixed trap size l with increasing the lattice size L. In particular, after some checks,

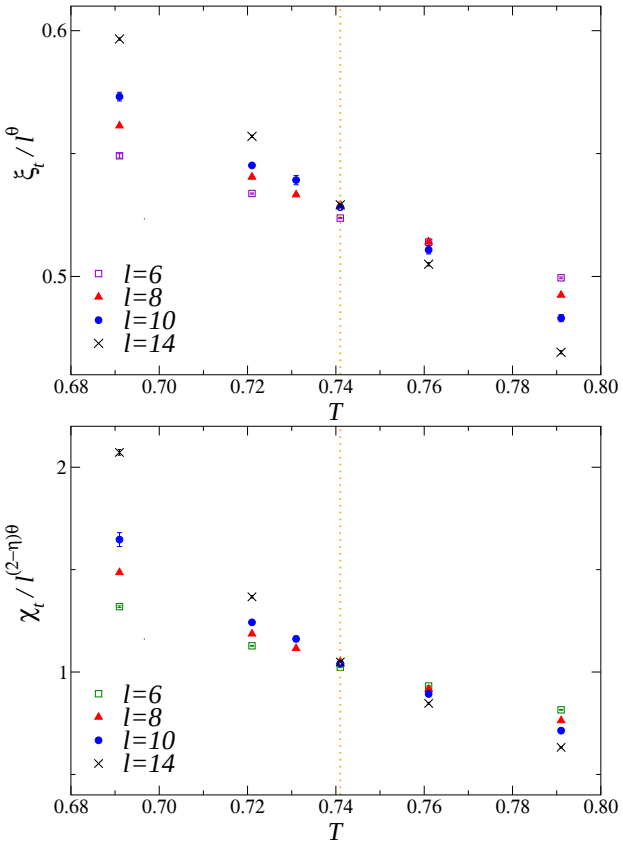

FIG. 10: (Color online) QMC data of ξ_t/l^θ (top) and $\chi_t/l^{(2-\eta)\theta}$ (bottom) in the presence of the trap. The vertical dotted line indicates the critical temperature $T_c = 0.7410$ obtained from the FSS analysis of Sec. III B.

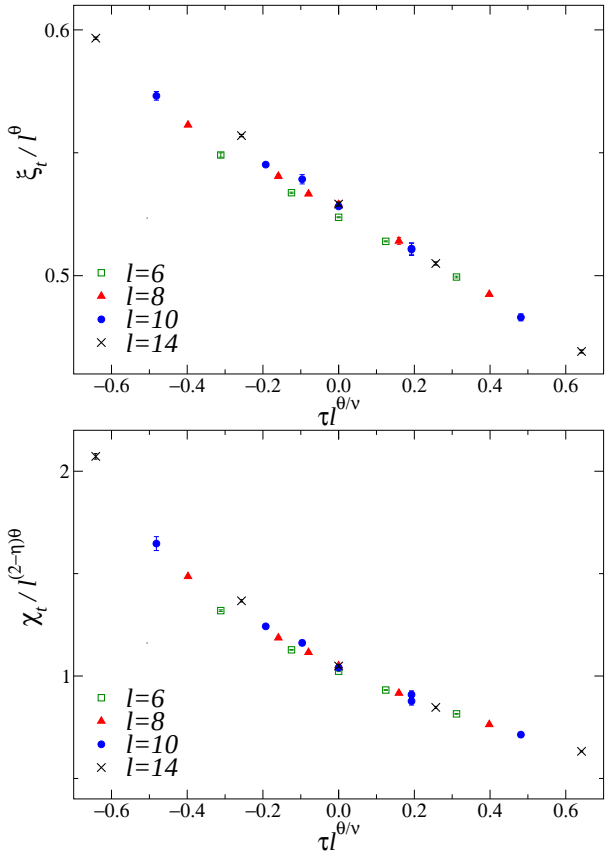

FIG. 11: (Color online) QMC data of ξ_t/l^θ (top) and $\chi_t/l^{(2-\eta)\theta}$ (bottom) in the presence of the trap vs $\tau l^{\theta/\nu}$ with $\tau \equiv T/T_c - 1$ and $T_c = 0.741$.

simulations up to $l = 10$ were generally performed taking $L = 4l + 1$, while for those at $l = 14$ we considered $L/l^\theta \gtrsim 7$. We return to this point below.

A. TSS analyses of QMC data

We now show that a TSS analysis of the data for trapped systems allows us to determine the critical parameters, analogously to the FSS analysis presented in the previous section.

In order to determine T_c from TSS, cf. Eqs. (17) and (18), we may exploit the fact that at $T = T_c$ (i.e. $\tau = 0$), the ratios $\chi_t/l^{\theta(2-\eta)}$ and ξ_t/l^θ become independent of the trap size l in the large-l limit. Therefore, we expect that sets of data for different trap sizes cross each other at one value of the temperature (apart from scaling corrections), providing an estimate of T_c, analogously to the FSS analysis of the previous section. This is indeed observed in Fig. 10, which shows the available data of $\chi_t/l^{\theta(2-\eta)}$ and ξ_t/l^θ versus T. The apparent crossing point of the TSS data indicates $T_c \approx 0.74$. A more accurate estimate is achieved by fitting the data to the simple Ansatz

$$a + b(T - T_c)l^{\theta/\nu}, \tag{37}$$

considering data sufficiently close to the crossing point to avoid higher powers of $\tau l^{\theta/\nu}$. We obtain $T_c = 0.741(2)$ and $T_c = 0.742(2)$ respectively from the data of ξ_t/l^θ and $\chi_t/l^{(2-\eta)\theta}$ (in both cases from data for $l \geq 8$). The error takes also into account results from different intervals of values of T around T_c. The expected $O(l^{-\omega\theta})$ scaling corrections, cf. Eq. (19), appear quite suppressed, at least for $l \geq 8$.

Although the available data come from moderately large trap sizes, their analysis shows a clear evidence of the expected TSS, which allows us to accurately estimate the critical temperature T_c with a precision of a few per mille, in good agreement with the estimate of T_c by the standard FSS analysis of Sec. III B, i.e. $T_c = 0.7410(1)$.

In Fig. 11 we plot the data of of $\chi_t/l^{\theta(2-\theta)}$ and ξ_t/l^θ versus $\tau l^{\theta/\nu}$. They are consistent with the scaling behavior predicted by Eqs. (17) and (18), approaching a universal curve in the large-l limit. The TSS of the one-particle correlation function $G_b(0, \mathbf{x})$ at T_c, i.e.

$$G_b(0, \mathbf{x}) = l^{-(1+\eta)\theta} g_b(X), \quad X \equiv r/l^\theta, \tag{38}$$

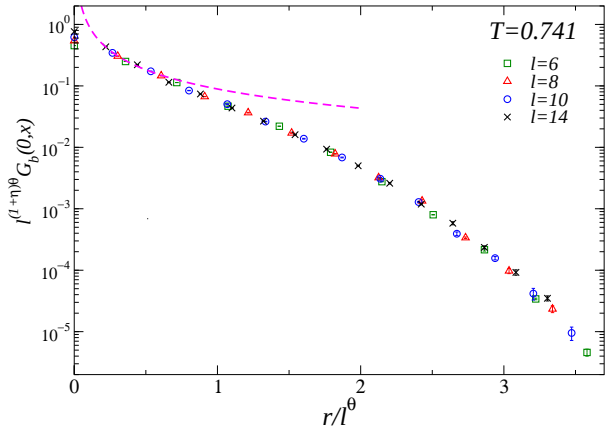

FIG. 12: (Color online) The one-particle correlation function $G_b(0,\mathbf{x})$ at T_c. The dashed line shows the expected small-distance behavior $G_b(0,\mathbf{x}) \sim r^{-(1+\eta)}$.

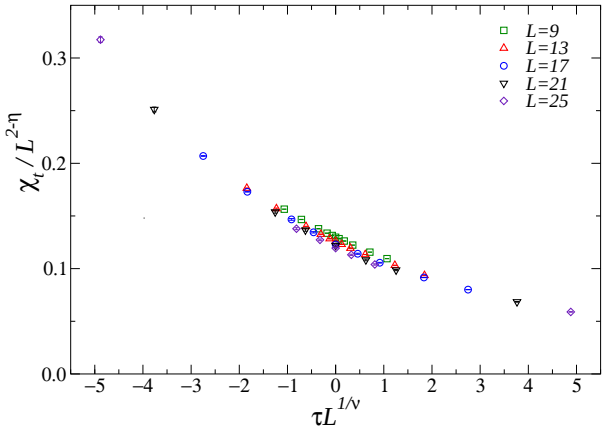

FIG. 13: (Color online) Finite-size scaling of the trap dependence of the QMC data of $\chi/L^{2-\eta}$ in the presence of the trap, from QMC simulations keeping $L/l^\theta = 2$ fixed and using open boundary conditions.

is nicely reproduced by the data shown in Fig. 12. At small distance r the two-point function G_b is expected to show the power-law behavior of the homogenous system, i.e. $G_b(0,\mathbf{x}) \sim 1/r^{1+\eta}$.

B. Finite-size effects with the trap

The finite-size effects in the presence of the trap, i.e. when considering the trap within a finite box of size L (with open boundary conditions), can be taken into account by adding a further dependence on $Ll^{-\theta}$ in the TSS Ansatz[31] (10), and in Eqs. (12) and (13) as well. For example the finite-size and trap-size scaling (FTSS) of the trap susceptibility χ_t and the correlation length ξ_t, cf. Eqs. (15) and (16), can be written as

$$\chi_t \approx L^{2-\eta} \mathcal{X}(\tau L^{1/\nu}, L/l^\theta), \tag{39}$$

$$\xi_t \approx L \mathcal{R}(\tau L^{1/\nu}, L/l^\theta). \tag{40}$$

The above scaling is confirmed by the data of χ_t shown in Fig. 13, obtained by QMC simulations keeping $L/l^\theta = 2$ fixed.

FTSS also implies that at T_c the ratio of quantities computed in box of size L becomes only function of L/l^θ asymptotically, i.e.,

$$s_\chi \equiv \frac{\chi_t(l,L)}{\chi_t(l, L\to\infty)} = f_\chi(L/l^\theta), \tag{41}$$

$$s_\xi \equiv \frac{\xi_t(l,L)}{\xi_t(l, L\to\infty)} = f_\xi(L/l^\theta). \tag{42}$$

Their data at T_c support this scaling behavior, see Fig. 14.

Moreover they tell us that around the transition the finite-size effects on χ_t and ξ_t get smaller than one per mille when $L/l^\theta \gtrsim 7$. All data reported in Sec. IV A, which were supposed to correspond to the infinite size limit, were obtained by simulations of systems satisfying this condition.

C. Trap-size dependence of the particle density

Finally, we discuss the trap-size dependence of the particle density, which has been considered in the literature as a possible probe of critical behavior, due to the experimental capability of measuring it quite accurately.

Analogously to the FSS of homogenous systems, the scaling behavior of the particle density is more involved, because it is dominated by an analytical contribution. In the presence of the trap, its behavior is further complicated by the fact that the particle density depends on the distance from the center of the trap.

To begin with, we consider the particle density at the center of the trap, $\mathbf{x} = 0$. Its asymptotic trap-size dependence is expected to be

$$\rho(0) = g_a(\tau) + l^{-y_n\theta} g_s(\tau l^{\theta/\nu}) + ..., \tag{43}$$

where $y_n\theta = 0.8664(3)$, g_a is a nonuniversal analytical function, and g_s is a scaling function. Moreover, the local-density approximation (LDA), see e.g. Refs. 4,37, suggests that the leading analytical term $g_a(\tau)$ is identical to that of Eq. (32) for homogenous systems. This is supported by the data at T_c shown in Fig. 15, which are consistent with the asymptotic formula

$$\rho(0) \approx \rho_0 + b\, l^{-y_n\theta}, \tag{44}$$

with ρ_0 equal to the leading constant term of homogenous systems, cf. Eq. (33) with $\rho_0 = 0.16187(1)$. Indeed, a linear fit of the data to Eq. (44) gives $\rho_0 = 0.1617(3)$ and $b = -0.027(1)$ with $\chi^2/\text{d.o.f.} \approx 0.4$.

Concerning the space-dependence of the particle density, and using rotational invariance, we expect that its large trap-size behavior is

$$\rho(\mathbf{x}) \approx f_a(r/l, T) + l^{-y_n\theta} f_s(r/l^\theta, \tau l^{\theta/\nu}), \tag{45}$$

where f_a is again an analytic function. Its analytic dependence on the ratio r/l is quite natural, because we

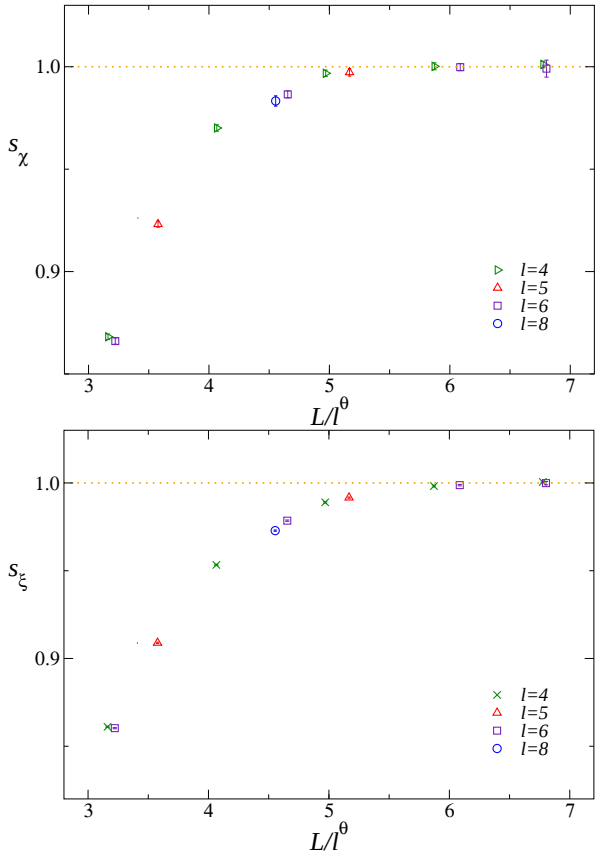

FIG. 14: (Color online) Finite-size scaling curves of the trap susceptibility χ_t and correlation length ξ_t at T_c, cf. Eqs. (41) and (42).

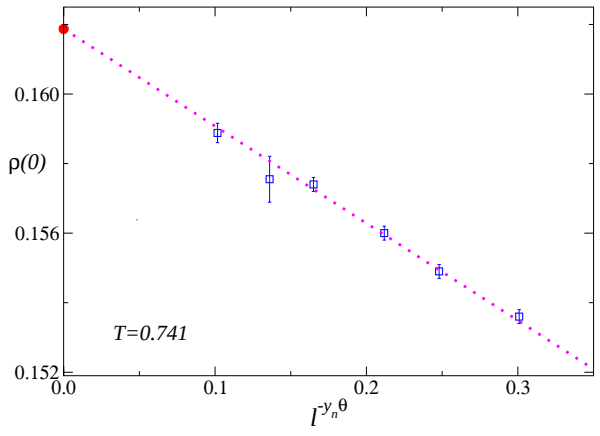

FIG. 15: (Color online) The particle density at T_c and at the center of the trap. The full circle along the y-axis shows the value $\rho_0 = 0.16187$ of the leading asymptotic term obtained for homogenous systems, see Fig. 6. The dotted line shows a linear fit to $\rho_0 + b\, l^{-\theta y_n}$, which gives $\rho_0 = 0.1617(3)$ and $b = -0.027(1)$.

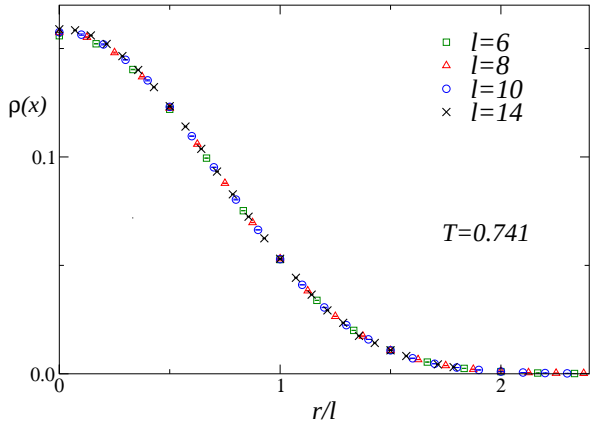

FIG. 16: (Color online) The space dependence of the particle density $\rho(x)$ at T_c in the presence of the trap.

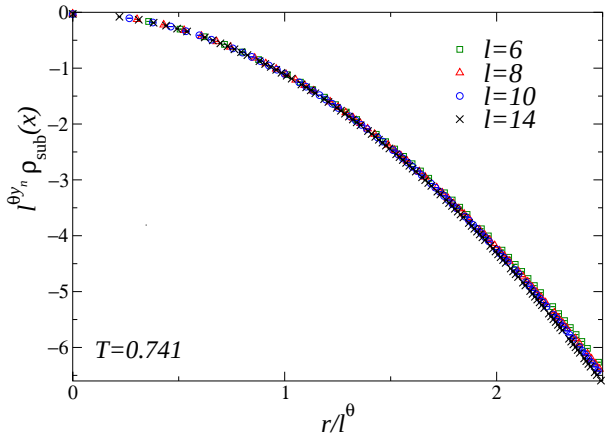

FIG. 17: (Color online) The subtracted particle density $\rho_{\rm sub}(x)$ at T_c, cf Eq. (50). The data of $l^{y_n\theta}\rho_{\rm sub}$ versus r/l^θ for different trap sizes collapse toward a unique curve, confirming the scaling behavior (50).

expect it to be a smooth function of

$$\mu_{\rm eff}(r/l) \equiv \mu - V(r) = \mu - (r/l)^2, \qquad (46)$$

as suggested by LDA. The asymptotic dependence on r/l is shown by the plot of Fig. 16. We expect that the leading analytic function $f_a(r/l, T)$ is provided by the LDA approximation, i.e. by the particle density $\rho_h(\mu_{\rm eff}, T)$ of the homogenous system in the infinite-volume limit. The asymptotic validity of the LDA of the particle density was also found at the $T = 0$ quantum transitions of 1D and 2D BH models[30,37,39].

The above results show that the behavior of the particle density around the center of the trap and across the transition is quite nontrivial. We finally write it as

$$\rho(\mathbf{x}) = \rho_h[\mu_{\rm eff}(r/l), T] + l^{-y_n\theta} f_s(r/l^\theta, \tau l^{\theta/\nu}). \qquad (47)$$

Let us consider the TSS limit at $T = T_c$ of this asymptotic behavior, i.e. $l \to \infty$ keeping $X \equiv r/l^\theta$ fixed. Since

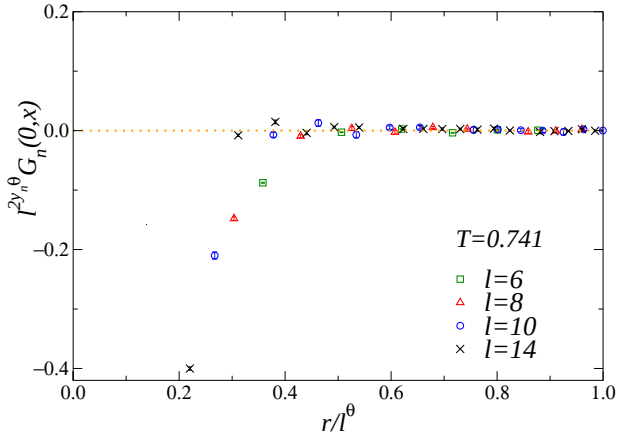

FIG. 18: (Color online) The density-density correlation $G_n(0,x)$ at T_c.

in this limit $r/l = X/l^{1-\theta} \to 0$, we can expand the analytical term, obtaining

$$\rho(\mathbf{x}) = \rho_h(\mu) + l^{-2(1-\theta)}\kappa_h(\mu)X^2 + O(l^{-4(1-\theta)}) + l^{-y_n\theta} f_s(X) + O(l^{-(y_n+\omega)\theta}), \quad (48)$$

where $\kappa_h(\mu) \equiv \partial\rho_{\rm h}(\mu)/\partial\mu$. Note that the $O(l^{-2(1-\theta)})$ term cannot be neglected with respect to the scaling term, because

$$2(1-\theta) < y_n\theta < 4(1-\theta). \quad (49)$$

Indeed, $2(1-\theta) = 0.8535(1)$ and $y_n\theta = 0.8664(3)$. Therefore, in order to determine the universal scaling term, we must subtract the terms containing $\rho_h(\mu)$ and $\kappa_h(\mu)$. They may be evaluated from calculations within the homogenous model at μ and T fixed, for example considering their large-L limit using periodic boundary conditions. Using the corresponding results at T_c for the FSS of homogenous systems, see Sec. III, we estimate $\rho_h(\mu = -2, T_c) \approx 0.16187$ and $\kappa_h(\mu = -2, T_c) \approx 0.90$. Then we define the subtracted particle density

$$\rho_{\rm sub}(\mathbf{x}) \equiv \rho(\mathbf{x}) - \rho_h(\mu,T) - l^{-2(1-\theta)}\kappa_h(\mu,T)X^2 \approx l^{-y_n\theta} f_s(X), \qquad X \equiv r/l^\theta. \quad (50)$$

Its scaling behavior is nicely confirmed by the corresponding data plotted in Fig. 17.

Finally in Fig. 18 we show our data for the particle-density correlation G_n, which vanish at relatively small distance, and do not apparently show scaling behaviors, likely because the trap size of the available data is still too small. Indeed the FSS data of Fig. 7 begin showing scaling at relatively large values of the size, essentially because the correlation function is significantly nonzero only at small distance.

V. CONCLUSIONS

We investigate the critical behavior of trapped particle systems at the finite-temperature superfluid transition driven by the formation of a Bose-Einstein condensate (BEC). In particular, we consider lattice particle systems described by the 3D Bose-Hubbard (BH) model (8), which is a realistic model of cold bosonic atoms in optical lattices[4,48]. We present FSS and TSS analyses of numerical QMC simulations of the homogenous and trapped 3D BH model in the hard-core $U \to \infty$ limit at fixed $\mu = -2$.

We show that an accurate study of the critical behavior, and accurate determinations of the critical parameters, can be achieved by matching the trap-size dependence of some appropriate observables with the scaling predicted by trap-size scaling (TSS), see e.g. Eqs. (12) and (18). The main advantage of this approach is that it is supposed to exactly converge to the critical parameters in the large trap-size limit, thus providing a systematic scheme to improve the results and control the uncertainty, without using further assumptions and approximations, such as mean-field and local-density approximation (LDA). Although the available QMC data are obtained for moderately large trap sizes, our TSS analysis allows us to accurately estimate the critical temperature T_c, e.g. $T_c = 0.741(2)$ from the analysis of the trap correlation length, cf. Eq. (16), which agrees with the critical value $T_c = 0.7410(1)$ obtained by a standard FSS analysis of QMC simulations of the homogenous 3D BH model.

Our numerical analysis may provide a guide for experimental investigations of finite-temperature and quantum transitions in physical systems that are made inhomogenoues by the presence of an external space-dependent field, like the experimentally interesting case of trapped atomic systems[3–5]. Indeed, it should show how the critical parameters may be determined by looking at the scaling of the critical modes with respect to the trap size, i.e. by matching the trap-size dependence of the experimental data with the expected TSS Ansatz, similarly to experiments probing the finite-size scaling behavior of homogenous ^{4}He systems at the superfluid transition[44].

A few comments are in order concerning the optimal observables to determine the critical parameters in trapped systems. Of course, they are those which are mostly determined by the critical modes around the center of the trap. In particular, the most convenient quantities are those whose leading behavior in the large trap-size limit is given by the universal TSS associated with the critical modes. In the case of the superfluid transition or BEC, the optimal quantities are related to the one-particle correlation function of the bosonic field around the center $\mathbf{x} = 0$ of the trap, which scales as $G_b(0,\mathbf{x}) \approx l^{-(1+\eta)\theta}\mathcal{G}_b(rl^{-\theta}, \tau l^{\theta/\nu})$. For example, we consider the trap susceptibility $\chi_t = \sum_{\mathbf{x}} G_b(0,\mathbf{x})$ and the trap correlation length ξ_t defined from the second moment of $G_b(0,\mathbf{x})$, which scale as $\chi_t \approx l^{(2-\eta)\theta}\mathcal{X}(\tau l^{\theta/\nu})$ and $\xi_t = l^\theta \mathcal{R}(\tau l^{\theta/\nu})$, respectively. Note that any length scale ξ extracted from the critical modes is expected to show the same TSS behavior as ξ_t, and therefore to be effective to determine the critical parameters.

Since the particle density can be accurately measured in experiments of trapped cold atoms, for example by *in situ* density image techniques[14,49,50], its behavior may be used as a probe of the critical behavior at finite-temperature and quantum transitions, see e.g. Refs. 19,24,26,32,33,36,41. The particle density turns out to show a more involved scaling behavior, given by Eq. (45). In this case the nontrivial TSS arising from the critical modes, which contains the information on the critical behavior, does not provide the leading contribution to the particle density. Indeed, it scales as $O(l^{-y_n\theta})$ with $y_n\theta \approx 0.866$, while the dominant contribution in the large trap-size limit is given by an analytical background function $f_a(r/l,T)$ related to noncritical modes, cf. Eq. (45). Our numerical analysis, see Sec. IV C, shows that such leading analytical background is well approximated (actually we conjecture that it is exactly given) by the corresponding LDA, i.e. by the infinite-volume limit of homogenous systems at chemical potential $\mu_{\rm eff} = \mu - V(r)$. Thus, TSS provides the leading behavior of the deviations from the LDA around the transition. Therefore, a careful subtraction is required in order to observe the genuine critical term which carries information on the critical temperature and the critical exponents. As a consequence, in order to infer the critical parameters from the particle density, very accurate experimental data are required to fit them to Eq. (45). Alternatively, one may resort to some approximations for the analytical background, but this may make the control of the real uncertainty more questionable, significantly affecting the accuracy of the results.

The particle-density correlations and compressibility are also working optical lattice observables, see e.g. Refs. 50,65,66. An analogous TSS applies to the connected particle-density correlation (4), for example $G_n(0,\mathbf{x}) \approx l^{-2\theta y_n}\mathcal{G}_n(rl^{-\theta},\tau l^{\theta/\nu})$. Thus information on the critical behavior can be achieved by matching the experimental data to this TSS Ansatz. However, our numerical analysis shows that the universal scaling of G_n at the superfluid transition turns out to appear at relatively small distance, see Fig. 7 and 18, which may make an accurate determination of its scaling quite hard.

As already mentioned, a promising quantity is the trap susceptibility $\chi_t \equiv \sum_{\mathbf{x}} G_b(\mathbf{0},\mathbf{x}) \sim l^{(2-\eta)\theta}$ with $(2-\eta)\theta \approx 1.12$, cf. Eqs. (15) and (17). However, we should note that χ_t is not proportional to the zero-momentum component of the momentum distribution, which is given by $n(\mathbf{k}) \equiv \sum_{\mathbf{x},\mathbf{y}} e^{i\mathbf{k}\cdot(\mathbf{x}-\mathbf{y})} G_b(\mathbf{x},\mathbf{y})$ even in the presence of the trap, and which can be experimentally related to the interference patterns of absorption images after a time-of-flight period in the large-time ballistic regime, see e.g. Ref. 4. Simple considerations show that $n(\mathbf{k})$, and in particular its zero-momentum component, is largely dominated by the noncritical regions of the trap, while the contribution of the critical modes are suppressed, roughly by a total volume factor of the system. Its critical scaling in trapped system in not clear, at least in the TSS framework, thus the global momentum distribution of the system does not appear promising to accurately determine the critical parameters. See, however, Refs. 12,22,26,41 for a discussion of methods based on the measurement of the momentum distribution.

We remark that the above considerations also apply to generic trapped interacting bosonic particle systems at the transition driven by BEC, such as the atomic system experimentally investigated in Ref. 6.

Let us finally mention that a substantial different TSS is expected in 2D trapped bosonic systems. The finite-temperature superfluid transition of 2D interacting bosonic systems is described by the Berezinskii-Kosterlitz-Thouless (BKT) theory[67,68], which is not associated with any spontaneous symmetry breaking and emergence of nonvanishing order parameter. Indeed, 2D fluids of identical bosons cannot undergo BEC, giving rise to a quasi-long range order at sufficiently low temperature, characterized by a power-law large-distance decay of the one-particle correlation function. Experimental evidences of superfluid transitions in trapped quasi-2D atomic gases have been reported in Refs. 69–73. Again, the trap gives rise to a substantial distortion of the BKT critical behavior of homogenous systems, see e.g. Ref. 41. The analysis of the BKT renormalizaton-group flow[74] shows that the asymptotic TSS at the BKT transition is characterized by an apparently trivial trap exponent $\theta = 1$, but the asymptotic behaviors show important multiplicative logarithms. For example, at T_c the trap correlation length is expected to increase as $\xi_t \sim l_t(\ln l_t)^\kappa$ with $\kappa = -1$ in the case of harmonic traps.

Acknowledgments

The QMC simulations were performed at the INFN Pisa GRID DATA center, using also the cluster CSN4. In total, simulations took approximately 50 years of CPU time on a single core of a recent standard commercial processor (most of them devoted to the simulations in the presence of the trap).

Appendix A: Derivation of the trap exponent θ

The *trap* exponent θ generally depends on the universality class of the transition, on the space dependence of the potential, and on the way it couples to the particles. In the case of 3D systems of interacting bosonic particles at the transition driven by the formation of BEC, the value of θ can be inferred by a renormalization-group (RG) analysis of the perturbation P_V representing the external trapping potential coupled to the particle density. Let us consider a generic trapping potential

$$V(r) = v^p r^p \tag{A1}$$

where p is a positive even interger number (in the case of a harmonic potential $p = 2$), with a trap size defined as

$l = J^{1/p}/v$. We follow the field-theoretical approach of Refs. 17,23, that is we consider the 3D Φ^4 quantum field theory which represents the 3D XY universality class, see e.g. Ref. 2,

$$H_{\Phi^4} = \int d^3x \left[|\partial_\mu \psi(\mathbf{x})|^2 + r|\psi(\mathbf{x})|^2 + u|\psi(\mathbf{x})|^4 \right], \quad \text{(A2)}$$

where ψ is the complex field associated with the order parameter, and r, u are coupling constants. Since the particle density corresponds to the energy operator $|\psi|^2$, we can write the perturbation P_V as

$$P_V = \int d^3x \, V(\mathbf{x}) |\psi(\mathbf{x})|^2. \quad \text{(A3)}$$

Introducing the RG dimension y_v of the constant v of the potential (A1), we derive the RG relation

$$p y_v - p + y_n = 3, \quad \text{(A4)}$$

where $y_n = 3 - 1/\nu$ is the RG dimension of the density/energy operator $|\psi|^2$. We eventually obtain

$$\theta = \frac{1}{y_v} = \frac{p\nu}{1 + p\nu}, \quad \text{(A5)}$$

which gives Eq. (11) in the case of a harmonic potential with $p = 2$. Note that Eq. (A5) formally gives $\theta = 1$ in the limit $p \to \infty$. This is consistent with the fact that the limit $p \to \infty$ corresponds to a homogenous system in a spherical box of size l, and open boundary conditions. Thus, TSS must reproduce the standard finite-size scaling of homogenous systems for $p \to \infty$, where the size $L = l$ behaves as a scaling field of dimension one in length units.

[1] K.G. Wilson, in *Nobel Lectures in Physics 1981-1990*, G. Ekspong Ed., World Scientific Publ., Singapore, 1993.
[2] J. Zinn-Justin, *Quantum Field Theory and Critical Phenomena* (Clarendon Press, Oxford, 1996).
[3] E.A. Cornell, C.E. Wieman, Rev. Mod. Phys. 74, 875 (2002); N. Ketterle, Rev. Mod. Phys. 74, 1131 (2002).
[4] I. Bloch, J. Dalibard, W. Zwerger, Rev. Mod. Phys. 80, 885 (2008).
[5] S. Giorgini, L.P. Pitaevski, S. Stringari, Rev. Mod. Phys. 80, 1215 (2008).
[6] T. Donner, S. Ritter, T. Bourdel, A. Öttl, M. Köhl, T. Esslinger, Science 315, 1556 (2007).
[7] K. Damle, T. Senthil, S.N. Majumdar, S. Sachdev, Europhys. Lett. 36, 7 (1996).
[8] S. Wessel, F. Alet, M. Troyer, G.G. Batrouni, Phys. Rev. A 70, 053615 (2004).
[9] M. Rigol and A. Muramatsu, Phys. Rev. A 70, 031603 (2004); Phys. Rev. A 72, 013604 (2005).
[10] S. Fölling, A. Widera, T. Müller, F. Gerbier, Q. Zhou, Phys. Rev. Lett. 97, 060403 (2006).
[11] Q. Niu, I. Carusotto, A.B. Kuklov, Phys. Rev. A 73, 053604 (2006).
[12] R.B. Diener, Q. Zhou, H. Zhai, T.L. Ho, Phys. Rev. Lett. 98, 180404 (2007).
[13] M. Holzmann, W. Krauth, Phys. Rev. Lett. 100, 190402 (2008).
[14] N. Gemelke, X. Zhang, C.-L. Hung, C. Chin, Nature 460, 995 (2009).
[15] A. Bezett, P.B. Blakie, Phys. Rev. A 79, 033611 (2009).
[16] E. Taylor, Phys. Rev. A 80, 023612 (2009).
[17] M. Campostrini, E. Vicari, Phys. Rev. Lett. 102, 240601 (2009); (E) 103, 269901 (2009).
[18] R.N. Bisset, M.J. Davis, T.P. Simula, P.B. Blakie, Phys. Rev. A 79, 033626 (2009).
[19] Q. Zhou, Y. Kato, K. Kawashima, N. Trivedi, Phys. Rev. Lett. 103, 085701 (2009).
[20] M. Rigol, G.G. Batrouni, V.G. Rousseau, R.T. Scalettar, Phys. Rev. A 79, 053605 (2009).
[21] I. Hen, M. Rigol, Phys. Rev. A 82, 043634 (2010).
[22] S. Trotzky, L. Pollet, F. Gerbier, U. Schnorrberger, I. Bloch, N.V. Prokofev, B. Svistunov, M. Troyer, Nat. Phys. 6, 998 (2010).
[23] M. Campostrini, E. Vicari, Phys. Rev. A 81, 023606 (2010); J. Stat. Mech.: Theory Exp. P08020 (2010); E04001 (2010).
[24] Q. Zhou, T-L Ho, Phys. Rev. Lett. 105, 245702 (2010).
[25] T.-L. Ho, Q. Zhou, Nat. Phys. 6, 131 (2010).
[26] L. Pollet, N.V. Prokof'ev, B.V. Svistunov, Phys. Rev. Lett. 104, 245705 (2010).
[27] L. Pollet, N.V. Prokof'ev, B.V. Svistunov, Phys. Rev. Lett. 105, 199601 (2010).
[28] S. Nascimbene, N. Nayon, F. Chevy, C. Salomon, New J. Phys. 12, 103026 (2010).
[29] Q. Zhou, Y. Kato, K. Kawashima, N. Trivedi, Phys. Rev. Lett. 105, 199602 (2010).
[30] M. Campostrini, E. Vicari, Phys. Rev. A 81, 063614 (2010); Phys. Rev. A 82, 063636 (2010).
[31] S.L.A. de Queiroz, R.R. dos Santos, R.B. Stinchcombe, Phys. Rev. E 81, 051122 (2010).
[32] S. Fang, C-M. Chung, P-N. Ma, D-W. Wang, Phys. Rev. A 83, 031605(R) (2011).
[33] X. Zhang, C.-L. Hung, S.-K. Tung, N. Gemelke, C. Chin, New J. Phys. 13, 045011 (2011).
[34] F. Crecchi, E. Vicari, Phys. Rev. A 83, 035602 (2011).
[35] K.W. Mahmud, E.N. Duchon, Y. Kato, N, Kawashima, R.T. Scalettar, N. Trivedi, Phys. Rev. B 84, 054302 (2011).
[36] K.R. Hazzard, E.J. Mueller, Phys. Rev. A 84, 013604 (2011).
[37] G. Ceccarelli, C. Torrero, E. Vicari, Phys. Rev. A 85, 023616 (2012).
[38] L. Pollet, Rep. Prog. Phys. 75, 094501 (2012).
[39] G. Ceccarelli, C. Torrero, Phys. Rev. A 85, 053637 (2012).
[40] Y. Khorramzadeh, Fei Lin, V.W. Scarola, Phys. Rev. A 85, 043610 (2012)
[41] J. Carrasquilla, M. Rigol, Phys. Rev. A 86, 043629 (2012).
[42] M.E. Fisher, M.N. Barber, D. Jasnow, Phys. Rev. A 8,

1111 (1973).
[43] J. Cardy, *Finite-Size Scaling*, North Holland, Amsterdam, 1988.
[44] F.M. Gasparini, M.O. Kimball, K.P. Mooney, M. Diaz-Avilla, Rev. Mod. Phys. 80, 1009 (2008).
[45] A. Pelissetto, E. Vicari, Phys. Rep. 368, 549 (2002).
[46] M. Hasenbusch, Int. J. Mod. Phys. C 12, 911 (2011).
[47] M.P.A. Fisher, P.B. Weichman, G. Grinstein, D.S. Fisher, Phys. Rev. B 40, 546 (1989).
[48] D. Jaksch, C. Bruder, J.I. Cirac, C.W. Gardiner, P. Zoller, Phys. Rev. Lett. 81, 3108 (1998).
[49] W. Bakr, J. Gillen, A. Peng, S. Foelling, M. Greiner, Nature 462, 74 (2009)
[50] C.-L. Hung, X. Zhang, L.-C. Ha, S.-K. Tung, N. Gemelke, C. Chin, New J. Phys. 13, 075019 (2011).
[51] B. Capogrosso-Sansone, N.V. Prokof'ev, B.V. Svistunov, Phys. Rev. B 75, 134302 (2007).
[52] S. Sachdev, *Quantum Phase Transitions* (Cambridge Univ. Press, 1999).
[53] R. Guida, J. Zinn-Justin, J. Phys. A 31, 8103 (1998).
[54] J.A. Lipa, D.R. Swanson, J.A. Nissen, T.C.P. Chui, U.E. Israelsson, Phys. Rev. Lett. 76, 944 (1996); J.A. Lipa, J.A. Nissen, D.A. Stricker, D.R. Swanson, T.C.P. Chui, Phys. Rev. B 68, 174518 (2003).
[55] M. Campostrini, M. Hasenbusch, A. Pelissetto, E. Vicari, Phys. Rev. B 74, 144506 (2006).
[56] E. Burovski, J. Machta, N. Prokof'ev, B. Svistunov, Phys. Rev. B 74, 132502 (2006).
[57] A.W. Sandvik, Phys. Rev. B 59, R14157 (1999).
[58] O.F. Syljuasen, A.W. Sandvik, Phys. Rev. E 66, 046701 (2002).
[59] In our QMC simulations the one-particle correlation function is computed using the method of A. Dorneich, M. Troyer, Phys. Rev. E 64, 066701 (2001).
[60] The helicity modulus Υ is related to the change of the partition function Z under twists ϕ of the boundary conditions along one of the lattice directions, i.e. $R_\Upsilon \equiv \Upsilon L = -\partial^2 \ln Z(\phi)/\partial\phi^2|_{\phi=0}$.
[61] A.W. Sandvik, Phys. Rev. B 56, 11678 (1997).
[62] E.L. Pollock, D.M. Ceperley, Phys. Rev. B 36, 8343 (1987).
[63] G.K. Campbell, J. Mun, M. Boyd, P. Medley, A.E. Leanhardt, L.G. Marcassa, D.E. Pritchard, W. Ketterle, Science 313, 649 (2006).
[64] T. Yefsah, R. Desbuquois, L. Chomaz, K.J. Günter, J. Dalibard Phys. Rev. Lett. 107, 130401 (2011).
[65] S. Foelling, F. Gerbier, A. Widera, O. Mandel, R.W. Hansch, I. Block, Nature 434, 481 (2005).
[66] I.B. Spielman, W.D. Phillips, J.V. Porto, Phys. Rev. Lett. 98, 080404 (2007).
[67] J.M. Kosterlitz, D.J. Thouless, J. Phys. C: Solid State 6, 1181 (1973)
[68] V.L. Berezinskii, Sov. Phys. JETP 34, 610 (1972).
[69] Z. Hadzibabic, P. Krüger, M. Cheneau, B. Battelier, J. Dalibard, Nature 441, 1118 (2006).
[70] P. Krüger, Z. Hadzibabic, J. Dalibard, Phys. Rev. Lett. 99, 040402 (2007).
[71] Z. Hadzibabic, P. Krüger, M. Cheneau, S.P. Rath, J. Dalibard, New J. Phys. 10, 045006 (2008).
[72] P. Cladé, C. Ryu, A. Ramanathan, K. Helmerson, W.D. Phillips, Phys. Rev. Lett. 102, 170401 (2009).
[73] C.-L. Hung, X. Zhang, N. Gemelke, C. Chin, Nature 470, 236 (2011).
[74] A. Pelissetto, E. Vicari, in preparation.